Engineering 18 (2022) 49–61

Contents lists available at ScienceDirect

Engineering

journal homepage: www.elsevier.com/locate/eng

Research
Unconventional and Intelligent Oil and Gas Engineering—Review

Probing the Interfacial Forces and Surface Interaction Mechanisms in Petroleum Production Processes

Diling Yang [a], Xuwen Peng [a], Qiongyao Peng [a], Tao Wang [a], Chenyu Qiao [a], Ziqian Zhao [a], Lu Gong [a], Yueliang Liu [b], Hao Zhang [a,*], Hongbo Zeng [a,*]

[a] Department of Chemical and Materials Engineering, University of Alberta, Edmonton, AB T6G 1H9, Canada
[b] College of Petroleum Engineering, China University of Petroleum, Beijing 102249, China

ARTICLE INFO

Article history:
Received 17 January 2022
Revised 22 April 2022
Accepted 17 June 2022
Available online 26 July 2022

Keywords:
Intermolecular and surface forces
Interface
Emulsion
Colloids
Fouling and antifouling
Water treatment

ABSTRACT

Despite the advances that have been made in renewable energy over the past decade, crude oil or petroleum remains one of the most important energy resources to the world. Petroleum production presents many challenging issues, such as the destabilization of complex oil–water emulsions, fouling phenomena on pipelines and other facilities, and water treatment. These problems are influenced by the molecular forces at the oil/water/solid/gas interfaces involved in relevant processes. Herein, we present an overview of recent advances on probing the interfacial forces in several petroleum production processes (e.g., bitumen extraction, emulsion stabilization and destabilization, fouling and antifouling phenomena, and water treatment) by applying nanomechanical measurement technologies such as a surface forces apparatus (SFA) and an atomic force microscope (AFM). The interaction forces between bitumen and mineral solids or air bubbles in the surrounding fluid media determine the bitumen liberation and flotation efficiency in oil sands production. The stability of complex oil/water emulsions is governed by the forces between emulsion drops and particularly between interface-active species (e.g., asphaltenes). Various oil components (e.g., asphaltenes) and emulsion drops interact with different substrate surfaces (e.g., pipelines or membranes), influencing fouling phenomena, oil–water separation, and wastewater treatment. Quantifying these intermolecular and interfacial forces has advanced the mechanistic understanding of these interfacial interactions, facilitating the development of advanced materials and technologies to solve relevant challenging issues and improve petroleum production processes. Remaining challenges and suggestions on future research directions in the field are also presented.

1. Introduction

Renewable energy, which is generated from renewable resources such as sunlight, tides, and waves, has attracted a great deal of attention—particularly over the past decade—and is unquestionably the primary energy source for the future of humankind. With the recent advances that have been made in new energy materials and technologies, renewable energy now contributes about 20% of the world's energy consumption, while fossil fuels still supply approximately 80% of the overall global energy consumption. Crude oil or petroleum is one of the most important types of fossil fuels. In September 2021, the Organization of the Petroleum Exporting Countries (OPEC) forecasted that global oil demand will grow drastically in the next few years due to economic recovery from the pandemic; it is then expected to plateau and most likely drop after 2035. Despite the petroleum industry's significant technological development more than a century, oil production processes still present challenging issues, such as the fouling of organic and inorganic species on pipelines and other devices, undesired stable oil/water emulsions in the various processes of oil production, and difficulty in separating oil from water and treating the process water or tailings water.

Taking oil sands production as an example, Canada has the third-largest oil resources (i.e., oil sands) in the world. Bitumen is liberated and extracted from oil sands by ① using warm water and then, through flotation and froth treatment processes, achieving oil/water/solid separation in surface mining operation;

* Corresponding authors.
E-mail addresses: hao.zhang@ualberta.ca (H. Zhang), hongbo.zeng@ualberta.ca (H. Zeng).

https://doi.org/10.1016/j.eng.2022.06.012

or ② using high-temperature steam via *in situ* extraction (e.g., steam-assisted gravity drainage (SAGD) recovery) [1–3]. During these extraction processes, undesired and stable saline water/oil emulsions and fine mineral solids tend to form and become trapped in the oil or water phase, resulting in fouling and corrosion phenomena on various instrument surfaces, as well as difficulties in oil/water separation, process water treatment and recycling, and tailings water treatment. These challenging interfacial phenomena are mainly driven and influenced by the molecular/surface forces of the various objects (e.g., different molecules, emulsion drops, and mineral particles) interacting at the oil/water/solid/gas interfaces in the relevant petroleum operations (Fig. 1). For example, the repulsive forces between stabilized emulsion drops or between fine particles in the surrounding fluid medium can stabilize oil or water drops and mineral solids, causing technical difficulties in removing saline water from oil products, separating oil from water, and cleaning the process water for cyclic use. Thus, characterizing and quantifying the intermolecular and surface forces involved are critical for a complete understanding of these challenging interfacial issues and of the underlying interfacial interaction mechanisms, which can facilitate the development of new materials, effective chemicals, and improved technologies to allow the oil industry to solve these challenges in oil production.

Several nanomechanical tools have been developed for measuring intermolecular and surface forces, such as the surface forces apparatus (SFA) [4–8], the atomic force microscope (AFM) [9], optical tweezer (OT) [10,11], the osmotic stress device [12], and the force balance [13]. Among these techniques, the SFA and AFM have been widely applied to measure the interaction forces of various molecules, particles, emulsion drops, gas bubbles, and substrates in complex fluids from the molecular level to the nano- and micro-scales [8,14–21]. Many studies have contributed to the quantification of interaction forces among different species in crude oil, such as asphaltenes, mineral particles, bitumen, air bubbles, and chemical additives (e.g., flocculants and antifoulants) [2,20,22–27]. In this work, we briefly review the basics of the typical interaction forces affecting different objects during oil production processes, the working principles of two commonly used nanomechanical tools (i.e., SFA and AFM), and how we applied these nanomechanical tools to directly probe the interfacial forces in selected petroleum production processes (e.g., oil extraction, emulsion treatment, fouling phenomena, and water treatment). Unresolved challenging problems and suggestions on future research directions are also discussed.

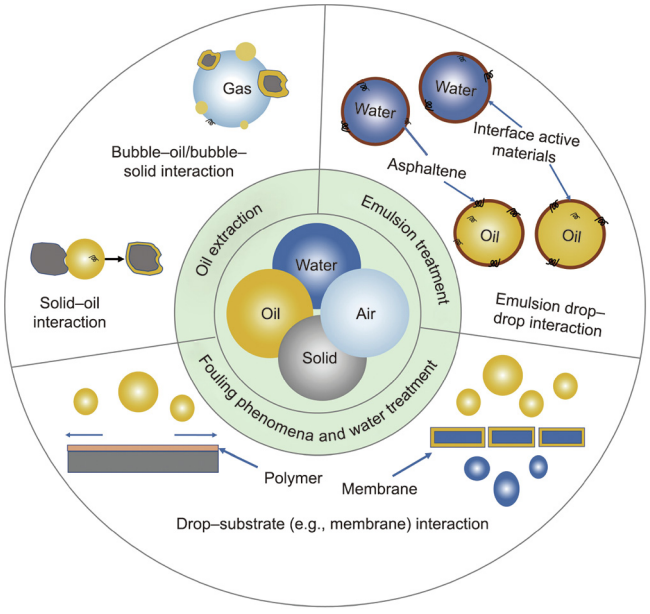

Fig. 1. Schematic illustration of different interactions among various components (e.g., emulsion drops, mineral solids, gas bubbles, and chemical additives) at the water/oil/solid/gas interfaces in selected petroleum operations (e.g., oil extraction, emulsion treatment, fouling and antifouling phenomena, and water treatment).

2. Experimental methodologies and theoretical model

Since the classical Derjaguin–Landau–Verwey–Overbeek (DLVO) theory was reported in the 1940s for describing the stability of colloids, many nanomechanical techniques have been developed and widely applied to measure the molecular and surface forces of different components, such as the SFA, AFM, and OT [8,28–30]. The SFA technique was pioneered by Tabor, Winterton, and Israelachvili in the late 1960s to early 1970s and was then modified and significantly advanced by Israelachvili. Since the 1970s, Israelachvili and coworkers have applied the SFA technique to quantify the physical forces (both normal and lateral forces) of a wide range of materials and biological systems in vapors and complex fluid media [6–8,31]. Many non-covalent interactions (e.g., van der Waals (VDW), electrical double layer (EDL), hydration, hydrophobic, cation–π, and anion–π interactions) were first experimentally quantified by using the SFA technique [6–8,26,31–35]. Fig. 2 provides an illustration of the setup for surface force measurements between two curved surfaces using the SFA, which are mounted in a crossed-cylinder configuration [36]. A picture of an SFA2000 chamber is shown in Fig. 2(a). The SFA can be used to directly quantify the forces of two interacting surfaces in vapors, organic media, or aqueous solution media that are correlated to the absolute separation distance [37]. This tool is particularly important for measuring the interaction forces of soft materials such as biopolymers, polymers, surfactants, and petroleum materials (e.g., asphaltenes and bitumen). In SFA measurements, the absolute separation distance and the surface deformation are determined through an optical technique called multiple beam interferometry (MBI) by monitoring the wavelength shifts of the fringes of equal chromatic order (FECOs), as shown in Figs. 2(b) and (c), which is generally difficult to achieve using other force measurement techniques [38]. The normal forces are determined using Hooke's law by monitoring the spring deflection based on the difference between the driven distance and the actual surface–surface separation change, as monitored using the FECO patterns. Taking asphaltenes as an example, the SFA can be used to measure the interactions between two asphaltene layers; between an asphaltene layer and a solid substrate surface or different coatings; or the interaction force changes between two substrate surfaces associated with the dynamic adsorption of asphaltenes from a solution medium, as illustrated in Fig. 2(d). Such experimental configurations can be directly adopted to measure the forces of other substances (e.g., surfactants, polymers, bitumen, and nanoparticles).

The AFM is another powerful nanomechanical tool that has been widely used for characterizing the nanoscopic surface topographic features of various materials and for measuring the molecular and surface forces in vapors or complex fluid media [30,39]. Fig. 3 provides an illustration of the working principles of the AFM [40]. Various AFM probes have been used for imaging and force measurements, including: a sharp tip, a colloid probe made by gluing a colloidal particle to a tipless cantilever, and bubble and drop probes made by attaching a gas bubble or liquid droplet to a tipless cantilever, as shown in Fig. 3 [16–18,41–49]. The colloid probe enables the surface force measurements of various particle materials (e.g., minerals, polymers, and cells). Further-

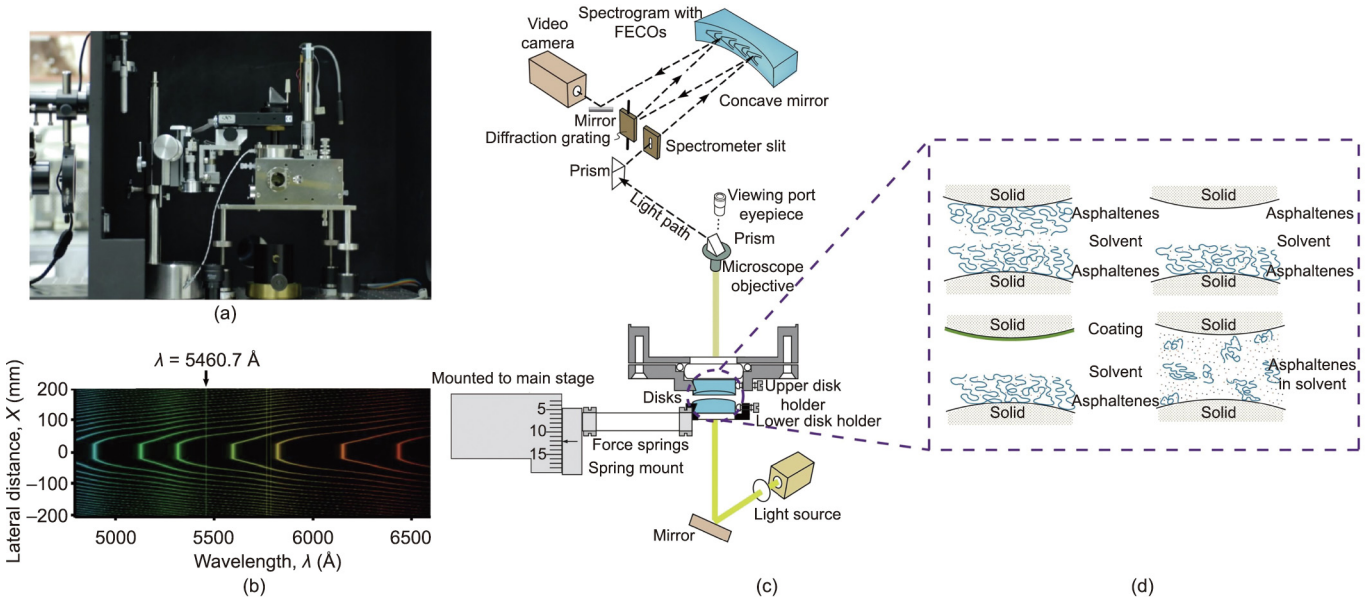

Fig. 2. Illustration of the setup for surface force measurements between two curved surfaces using the SFA. (a) Picture of a SFA2000 chamber. (b) Typical picture of the FECOs obtained using MBI, corresponding to the interaction position when two curved surfaces are in contact. (c) Schematic of the sample alignment and light path in a typical SFA measurement. (d) Four commonly used experimental configurations for quantifying the forces of asphaltenes versus asphaltenes (asphaltenes are used as a model material for illustration), asphaltenes versus a solid substrate, asphaltenes versus a coating, and two solid surfaces associated with the dynamic adsorption of asphaltenes. Reproduced from Ref. [36], with permission.

more, the more recently developed bubble/drop probe techniques allow researchers to directly quantify the interaction forces of highly deformable objects such as water-in-oil or oil-in-water emulsions and the gas bubbles commonly present in petroleum production and other engineering processes. Recently, we coupled the colloid/drop/bubble probe AFM technique with reflective interferometry, achieving simultaneous measurements of surface forces and monitoring of the nanoscopic spatiotemporal evolution of the confined thin liquid film of bubbles, drops, colloids, and substrates [50,51]. When measuring the forces using an AFM, a sharp AFM tip or a colloid/bubble/drop probe is placed on top of the desired sample and is then driven to approach the sample until the cantilever reaches a desired deflection with a selected contact time. The cantilever is then driven to move away from the sample to finish the approaching–separation force measurement cycle [52,53]. The interaction forces are determined based on Hooke's law by monitoring the deformation of the AFM cantilever (acting as a force spring), using a quartered photodiode to detect the laser reflection from the back side of the cantilever (Fig. 3) [40].

Force–distance profiles obtained from experimental measurements using nanomechanical tools generally need to be theoretically analyzed through colloidal interaction models, which provide useful information on the properties of the interacting materials and their interaction mechanisms. In a typical petroleum production process, many interaction forces—such as the VDW, EDL, and hydrophobic interactions—can influence the interaction behaviors of the different components involved [54]. VDW and EDL interactions are generally depicted by the classical DLVO theory [55]. VDW forces are widely present in various materials and engineering systems, and the VDW forces of macroscopic objects of different geometries can be derived using the Hamaker approach or, more rigorously, using the Lifshitz theory [51,55]. For the VDW interactions of two planar surfaces, the VDW force per unit area ($\prod_{VDW}$) also known as the VDW disjoining pressure) is given by Eq. (1), where A_H is the so-called Hamaker constant for two objects in a surrounding medium (e.g., an aqueous solution) and h is their separation distance.

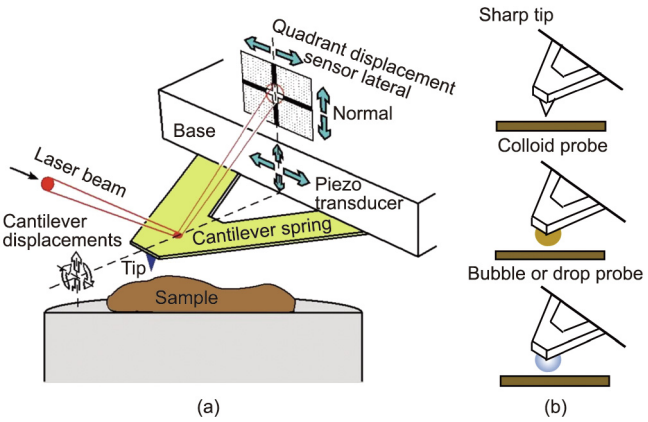

Fig. 3. (a) Schematic of a typical experiment setup for imaging surface topography at the nano-scale or for force measurements using a sharp nano tip with an AFM. (b) Three commonly used AFM probes. Reproduced from Ref. [40] with permission.

$$\prod_{VDW} = -\frac{A_H}{6\pi h^3} \quad (1)$$

Another important interaction is the EDL force, which is strongly dependent on the salinity, pH, ion type, pH of the aqueous media, and surface charge properties of the interacting objects. For material systems of different geometries, the equations for the EDL interactions are in different mathematical forms [39,55]. The EDL forces of two parallel flat surfaces per unit area ($\prod_{EDL}$) are given by Eqs. (2) and (3) for the constant potential and constant charge cases, respectively [30,55], where κ is the inverse Debye length, ε_0 is the vacuum permittivity, ε is the dielectric constant of the aqueous solution, ψ_1 and ψ_2 are the respective surface potentials of materials 1 and 2, and σ_1 and σ_2 are the respective surface charge densities of materials 1 and 2 [55]. For the interactions of two curved surfaces, the VDW and EDL interactions are related to the interaction energy of two parallel planar surfaces through the Derjaguin approximation [30,55].

$$\prod_{\mathrm{EDL}} = \frac{2\varepsilon_0\varepsilon\kappa^2\left[\left(\mathrm{e}^{+\kappa h}+\mathrm{e}^{-\kappa h}\right)\psi_1\psi_2-\left(\psi_1^2+\psi_2^2\right)\right]}{\left(\mathrm{e}^{+\kappa h}-\mathrm{e}^{-\kappa h}\right)^2} \quad \text{(constant potential case)} \tag{2}$$

$$\prod_{\mathrm{EDL}} = \frac{2}{\varepsilon_0\varepsilon}\left[\sigma_1\sigma_2\mathrm{e}^{-\kappa h}+\left(\sigma_1^2+\sigma_2^2\right)\mathrm{e}^{-2\kappa h}\right] \quad \text{(constant charge case)} \tag{3}$$

For a symmetric configuration, the two surfaces are of the same material, and the above two equations can be simplified to Eqs. (4) and (5), respectively.

$$\prod_{\mathrm{EDL}} = \frac{2\varepsilon_0\varepsilon\kappa^2\psi^2\left[\left(\mathrm{e}^{+\kappa h}+\mathrm{e}^{-\kappa h}\right)-2\right]}{\left(\mathrm{e}^{+\kappa h}-\mathrm{e}^{-\kappa h}\right)^2} \quad \text{(constant potential case)} \tag{4}$$

$$\prod_{\mathrm{EDL}} = \frac{2\sigma^2\mathrm{e}^{-\kappa h}}{\varepsilon_0\varepsilon}\left(1+2\mathrm{e}^{-\kappa h}\right) \quad \text{(constant charge case)} \tag{5}$$

In the early 1980s, Israelachvili and Pashley [32] experimentally quantified the hydrophobic interactions of two hydrophobic surfaces in aqueous media via the self-assembly of two surfactant monolayers using an SFA. The correlation between the hydrophobic interaction force per unit surface area ($\prod_{\mathrm{HB}}$) and the separation distance was proposed to be exponential, given by Eq. (6) for two parallel planes, where C_0 is a constant (unit: $\mathrm{N{\cdot}m^{-1}}$) relevant to the surface wettability of the objects, and D_0 is the decay length of hydrophobic (HB) interaction.

$$\prod_{\mathrm{HB}} = -\frac{C_0}{D_0}\mathrm{e}^{-\frac{h}{D_0}} \tag{6}$$

For interactions involving highly deformable liquid droplets and gas bubbles, under the influence of the interaction forces, the surfaces of droplets or bubbles readily deform while the confined liquid film drains off between the objects. The Stokes–Reynolds–Young–Laplace (SRYL) model, which couples the Stokes–Reynolds lubrication equation and the augmented Young–Laplace equation, has been commonly used to analyze the interaction process and the force results obtained [56,57]. The Stokes–Reynolds lubrication equation, given by Eq. (7) [58–61], describes the thin liquid film drainage between two interacting surfaces, where $h(r,t)$ is the confined liquid film thickness, r is the distance between a selected position and the bubble central axis, t is time, μ is the dynamic viscosity of the surrounding liquid, and $p(r,t)$ is the excessive hydrodynamic pressure in the confined liquid film (as compared with the bulk liquid).

$$\frac{\partial h(r,t)}{\partial t} = \frac{1}{12\mu r}\frac{\partial}{\partial r}\left(rh^3\frac{\partial p(r,t)}{\partial r}\right) \tag{7}$$

The augmented Young–Laplace equation describes the surface deformation of bubbles or drops by including the effects of disjoining pressure. Eqs. (8–10) show the augmented Young–Laplace equation for the interactions of gas bubbles or liquid droplets in different configurations, where R_{b} is the bubble/drop radius, R_{p} is the particle radius, $R_{\mathrm{bp}} = (1/R_{\mathrm{b}} + 1/R_{\mathrm{p}})^{-1}$, γ is the interfacial tension, and $\Pi[h(r,t)]$ is the total disjoining pressure [39,55,59,62].

$$\frac{\gamma}{2r}\frac{\partial}{\partial r}\left(r\frac{\partial h(r,t)}{\partial r}\right) = \frac{2\gamma}{R_{\mathrm{b}}} - p(r,t) - \prod[h(r,t)] \quad \text{(bubble/drop—bubble/drop)} \tag{8}$$

$$\frac{\gamma}{r}\frac{\partial}{\partial r}\left(r\frac{\partial h(r,t)}{\partial r}\right) = \frac{2\gamma}{R_{\mathrm{b}}} - p(r,t) - \prod[h(r,t)] \quad \text{(drop/bubble—plane)} \tag{9}$$

$$\frac{\gamma}{r}\frac{\partial}{\partial r}\left(r\frac{\partial h(r,t)}{\partial r}\right) = \frac{2\gamma}{R_{\mathrm{bp}}} - p(r,t) - \prod[h(r,t)] \quad \text{(drop/bubble—spherical particle)} \tag{10}$$

The total disjoining pressure usually arises from different interactions such as the VDW, EDL, hydrophobic, and steric interactions involved in the interacting systems, as shown in Eq. (11):

$$\prod[h(r,t)] = \prod_{\mathrm{VDW}} + \prod_{\mathrm{EDL}} + \prod_{\mathrm{HB}} + \ldots \tag{11}$$

The overall interaction forces can be described by Eq. (12) [47]:

$$F(t) = 2\pi\int_0^{\infty}\left[p(r,t)+\prod\left(h(r,t)\right)\right]r\mathrm{d}r \tag{12}$$

3. Oil extraction

Depending on the geological conditions of the oil reservoirs and oil properties (e.g., light, medium, or heavy oil), oil is extracted or recovered by the petroleum industry using various methods. Conventional crude oil is in a liquid form under atmospheric conditions; it is generally extracted from underground oil reservoirs through drilling and pumping. In contrast, heavy bitumen generally cannot be readily extracted using traditional drilling and pumping technology. For example, the Canadian oil sands, which are one of the largest crude oil deposits on earth, are a mixture of crude bitumen (very heavy crude oil), mineral solids (e.g., silica sand and clay minerals), and water. The oil sands industry has been extracting and producing bitumen by either using open-pit mining technology for reserves up to 75 m deep—which consists of large-scale excavation, crushing, mixing with warm water, hydrotransport (liberation), flotation, and froth treatment processes—or using *in situ* extraction methods such as the SAGD recovery method by injecting high-temperature steam into oil sands deposits (mostly more than 200 m deep). As the warm-water-based open-pit mining method results in challenging tailings water issues, the oil industry has also explored the feasibility of other extraction technologies, such as non-aqueous extraction methods involving organic solvents. In the water-based bitumen-extraction processes, the interactions among bitumen, mineral solids, air bubbles, and the surrounding fluid media (i.e., water and organic solvents) significantly determine the efficiency of the abovementioned large-scale industrial interfacial processes. Thus, quantifying these interaction forces and understanding the underlying interfacial interaction mechanisms are of both fundamental and practical importance in developing more efficient and controllable oil-extraction processes and technologies.

The interactions between bitumen and mineral solids can be significantly influenced by the surrounding solvents (i.e., good or poor solvents of bitumen). In a previous work [16], we investigated the effects of two typical solvents—namely, cyclohexane (a good solvent for bitumen) and *n*-heptane (a poor solvent)—on the interactions of bitumen and mineral solids using an AFM. The force results were then correlated to the stabilization and removal of small bitumen-coated mineral particles in the oil phase. A colloid probe was prepared using a tipless cantilever with a spherical silica particle attached, as illustrated in Fig. 4(a). Figs. 4(b) and (c) show the typical interaction force profiles of a bare silica particle and a bitumen surface in cyclohexane and heptane, respectively. In cyclohexane, when the silica particle moved toward the bitumen-coated substrate, a relatively long-range repulsive force was measured, which became stronger as the two surfaces got closer; only a very weak attraction was detected during the separation of the two surfaces. In heptane, during the approaching process, the "jump-in" phenomenon was detected between the silica particle and bitumen surface at a distance D of approximately

3 nm; during the retraction or separation process, jump-out behavior was observed and a normalized attraction F_{ad}/R = 0.15 mN·m^{-1} was measured, where F_{ad} is adhesion force, R is particle radius. As bitumen dissolves well in cyclohexane, the substrate-supported bitumen was very swollen with the solvent, causing strong steric repulsion and hindering the attachment of the silica particle and bitumen surface. In contrast, bitumen has poor solubility in heptane and exhibited very limited swelling, leading to weak steric interaction; therefore, the attractive VDW interaction between silica and bitumen resulted in jump-in behavior at D of approximately 3 nm. To more systematically characterize the effects of the organic solvent on the interaction between silica solids and bitumen, their interaction forces were measured in various mixtures of cyclohexane and heptane. The cyclohexane volume fraction φ_c was varied from 1.00 (pure cyclohexane), to 0.75, 0.50, 0.25, and 0 (pure heptane). The adhesion results F_{ad}/R of the different cases are summarized and shown in Fig. 4(d). The normalized adhesion F_{ad}/R was greatly increased as the volume fraction of the good solvent cyclohexane, φ_c, decreased, indicating that the bitumen–silica attraction was clearly enhanced. In regard to the interactions of silica and bitumen in pure cyclohexane (i.e., a volume fraction of φ_c = 1.00), strong and long-ranged repulsive forces were measured in the approach process, which were contributed by the steric interaction of the swelling bitumen on opposing surfaces, as shown in Fig. 4(e). When the volume fraction was φ_c = 0 (i.e., pure heptane), an obvious attraction was detected during the approach process, which was due to the attractive VDW interactions between the shrunken (i.e., non-swelling) bitumen layers caused by the poor solvent, as shown in Fig. 4(f).

Using the same methodology as above, the surface forces were measured for the bitumen–bitumen case (one coated on a flat silica substrate, and the other coated on a silica microsphere probe). It was found that the adhesion detected during the separation process between the two bitumen surfaces was gradually

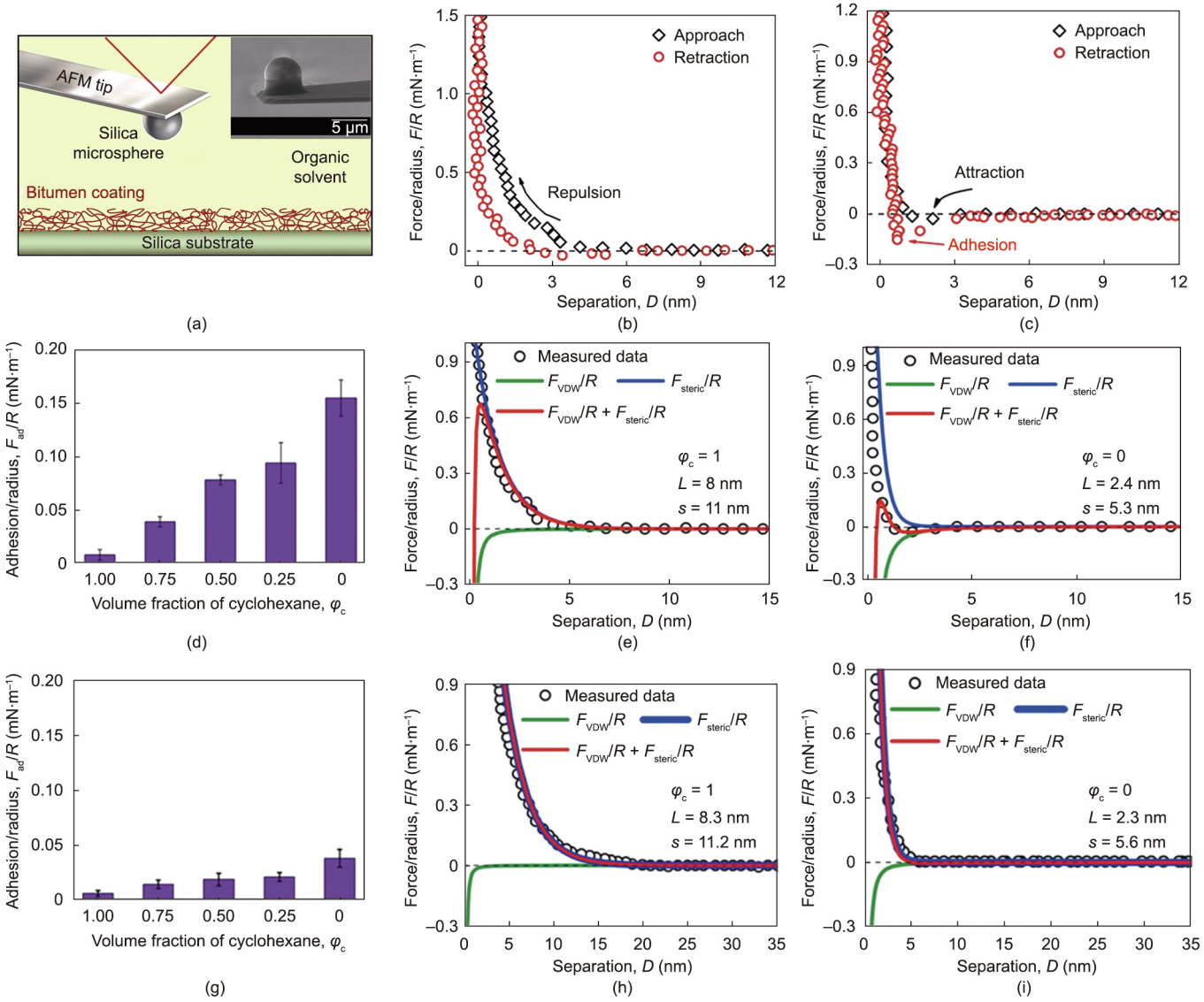

Fig. 4. (a) Illustration of surface force measurements using a colloid probe on an AFM and a scanning electron microscope (SEM) image of a silica particle attached to a tipless cantilever. (b, c) Experimental force results between silica particles and bitumen surfaces in (b) cyclohexane and (c) heptane. (d) The adhesion F_{ad}/R measured between silica and bitumen under various cyclohexane–heptane volume fraction conditions. (e, f) Measured interaction forces (black symbol) and theoretical analysis results (solid curve) for silica and bitumen in (e) pure cyclohexane (φ_c = 1.00) and (f) pure heptane (φ_c = 0). (g) The adhesion F_{ad}/R measured between two bitumen surfaces under different cyclohexane–heptane volume fraction conditions. (h, i) Experimental results (black symbol) and theoretical analysis (solid curve) for the interaction forces of two bitumen surfaces in (h) pure cyclohexane (φ_c = 1.00) and (i) pure heptane (φ_c = 0), where L and s are the fitted length of bitumen chains and the average spacing between two grafted points of bitumen chains, respectively, based on the Alexander–de Gennes steric model. Reproduced from Ref. [16] with permission.

increased in the cyclohexane–heptane mixtures as the volume fraction of the good solvent cyclohexane, φ_c, decreased, as shown in Fig. 4(g). The interaction profiles were also compared in more detail. For example, the range of repulsion measured during the approach of the two bitumen surfaces was much longer in the good solvent (i.e., cyclohexane) than in the poor solvent (i.e., heptane). Moreover, it was found that the repulsion started at a separation of about 8 nm for the asymmetric silicon–bitumen configuration, while repulsion was detected at a separation of about 16 nm for the symmetric interaction of two bitumen surfaces. Thus, we propose that bitumen molecules are in more extended conformations in a relevantly good solvent such as cyclohexane, which results in significant repulsive forces during an approach and weak adhesion during a separation due to the steric forces between the swollen surfaces. In comparison, in pure heptane, the enhanced adhesion is mainly due to VDW attraction and to the interpenetration of bitumen molecules at the contact interface. It is notable that the experimental results agree well with the theoretical analysis on the surface forces, when the contributions from the VDW and steric interactions are included (Figs. 4(e), (f), (h), and (i)). These results improve the fundamental understanding of the oil–solid and oil–oil interaction mechanisms in oil extraction, as well as the interaction mechanism of small solid particles suspended in the oil phase (e.g., crude oil and diluted bitumen). These findings are also of great significance for the development of an effective economic strategy to remove the fine particles in bitumen extraction during petroleum production.

During bitumen aeration, or the so-called bitumen flotation process, liberated bitumen is aerated to float to the upper region of the fluid, which is a very important step for collecting the bitumen product and determining the bitumen recovery and product quality [2]. Hence, it is very important to determine the interaction mechanisms among the air bubbles and bitumen under various solution conditions and investigate the effects of environmental conditions. Over the past few years, several studies—mainly by our research lab—have characterized the interaction forces involving bitumen, asphaltenes, solid surfaces, and gas bubbles using SFA and AFM techniques. We have found that the interaction forces are strongly dependent on the solution conditions (e.g., pH, salt type, and salinity in aqueous media). In one of our previous studies, we directly measured the surface forces of air bubbles and bitumen by employing the bubble probe AFM technique and revealed the important effects of ions and solution pH on their interactions by analyzing the force profiles using the SRYL model [19]. A typical experiment setup using the bubble probe AFM is illustrated in Fig. 5(a). The morphologies of the bitumen surfaces under various ion concentrations and pH conditions were characterized. The bitumen surface showed a root mean square (RMS) roughness of 0.53 nm under low salinity (1 mmol·L^{-1} NaCl) at pH 4.0 (Fig. 5(b)). Surface force measurements showed that air bubbles could not attach to bitumen surfaces during the approach process in 1 mmol·L^{-1} NaCl (pH 4.0), as shown in Fig. 5(c); this was because the repulsive VDW interactions and long-range repulsive EDL forces (with a Debye length of 9.6 nm) could overcome the attractive hydrophobic interactions of the bubble–water–bitumen system. The bitumen surface becomes evidently rougher (RMS roughness = 1.28 nm) under high salinity conditions (500 mmol·L^{-1} NaCl, pH 4.0) (Fig. 5(d)), and the surface RMS roughness increased from 1.28 to 1.50 nm and then to 2.07 nm as the solution pH increased from 4.0 to 5.8 and then to 8.5, respectively, in 500 mmol·L^{-1} NaCl (Figs. 5(d)–(f)). We observed more aggregates as the solution pH and salt concentration increased. Such phenomena are likely to be caused by ① weakened electrostatic repulsion of relevant groups on interfacial bitumen molecules under high salt concentration conditions; and ② deprotonation of relevant groups and conformation changes of interfacial bitumen molecules under elevated pH conditions [20,63].

During the force measurements, in a higher salinity solution (i.e., 500 mmol·L^{-1} NaCl), air bubbles jumped into contact with bitumen surfaces during the approach under all the pH conditions tested, as shown in Figs. 5(g)–(i). In 500 mmol·L^{-1} NaCl, the EDL repulsion was greatly weakened (with a Debye length of less than 1 nm) and the VDW interactions remained repulsive; thus, hydrophobic attraction played a critical role in the bubble–bitumen attachment behavior. Through a theoretical analysis using the SRYL model, the decay length of the hydrophobic interaction was determined to be D_0 = (0.95 ± 0.05), (0.78 ± 0.05), and (0.65 ± 0.07) nm for pH 4.0, 5.8, and 8.5, respectively (Figs. 5(g)–(i)). The weakening of the hydrophobic interaction was probably caused by the deprotonation of some of the polar groups of the interface-active molecules in the alkaline environment.

The influence of divalent cations (e.g., calcium ions) on the bitumen surface behavior (e.g., morphology) and on the surface forces between bubbles and bitumen was also investigated. In an aqueous solution of 500 mmol·L^{-1} NaCl (pH 8.5) with 10 mmol·L^{-1} $CaCl_2$, the morphologies of the bitumen surface exhibited an RMS roughness of 4.28 nm (Fig. 5(j)), and air bubble–bitumen "jump-in" behavior was detected during the approach process in force measurements. In this case, the decay length of hydrophobic interaction was found to be D_0 = (1.20 ± 0.10) nm (Fig. 5(k)). The increased surface roughness is likely to be due to local aggregation caused by calcium ion-induced bridging (via interactions with carboxyl groups), leading to more hydrophobic domains facing the aqueous solution and thus strengthening the apparent hydrophobic air bubble–bitumen attraction. These quantitative measurements reveal the nanoscopic air bubble–bitumen interaction mechanisms, which can be applied in order to better modulate and improve the relevant petroleum production processes.

4. Emulsion treatment

Water-in-oil, oil-in-water, and even more complex (e.g., water-in-oil-in-water, oil-in-water-in-oil) emulsions commonly exist in various petroleum production processes. Stable emulsions are generally undesired in the petroleum industry, as they can cause technical challenges such as difficulty separating oil and water, fouling, and corrosion issues (due to the presence of ions such as Cl^-). Understanding the interaction mechanisms of the emulsions in petroleum production is of great importance for developing effective approaches for demulsification and enhancing oil/water separation. Direct quantification of the molecular/surface forces of the different objects involved in the emulsion interactions in petroleum engineering has long been experimentally difficult, particularly at the molecular or nanoscopic scale, and could not be achieved until advances were made in nanomechanical technologies such as the SFA and AFM. The experimental difficulties were mainly due to the complex chemical composition of crude oil, as well as the highly deformable oil/water interfaces of the emulsions; it was very challenging to experimentally correlate the forces, deformation of surfaces, and separation distance during emulsion interactions. The development of the bubble/drop probe AFM technique and its coupling with reflection interference contrast microscopy (RICM) have made it experimentally feasible to simultaneously probe surface forces with better than nanonewton-scale resolution and measure the spatiotemporal evolution (i.e., drainage dynamics) of confined thin liquid films down to nanometer-scale thickness for the interactions of highly deformable emulsion drops and bubbles. In this section, we

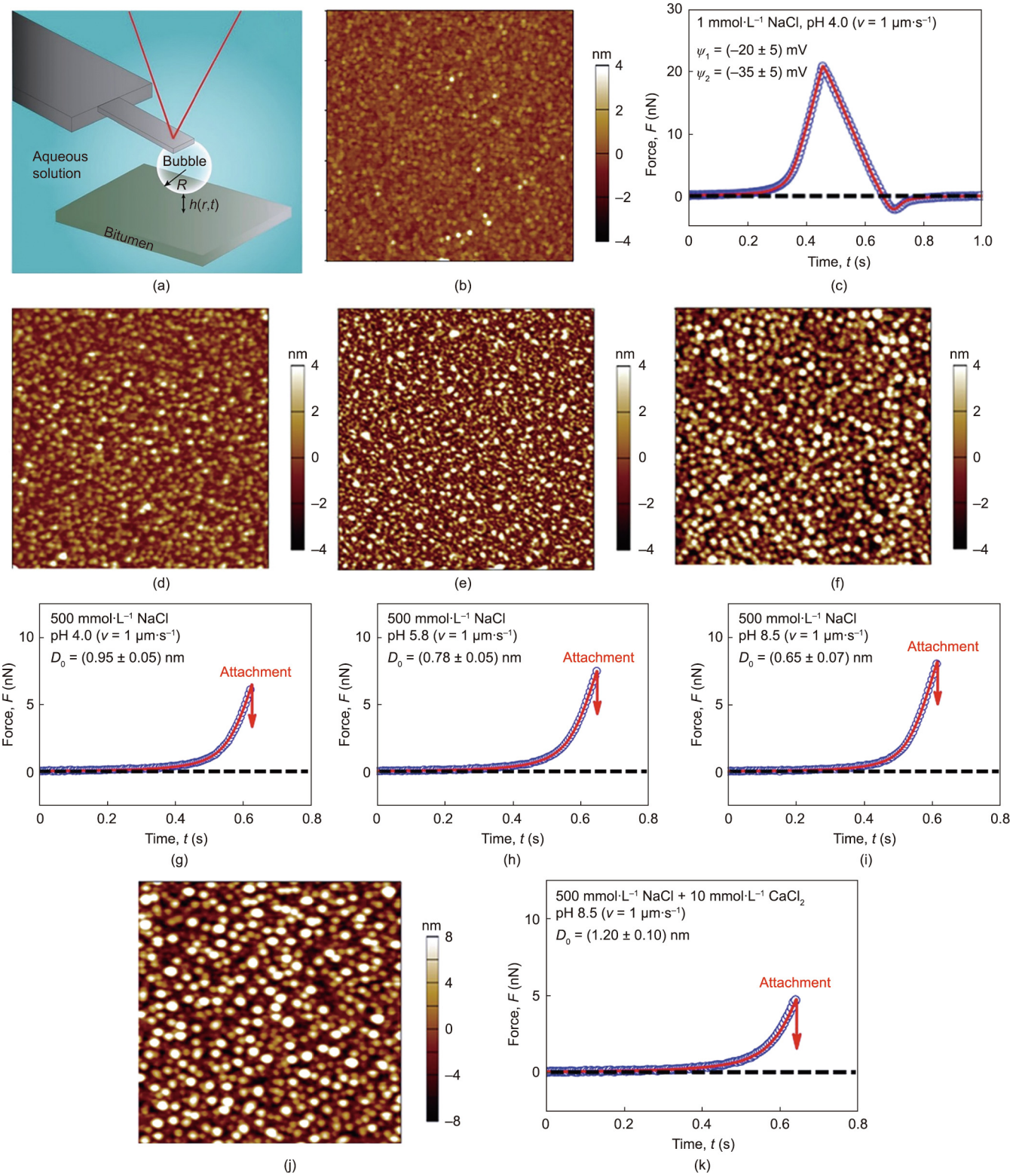

Fig. 5. (a) Illustration of AFM force measurements using a bubble probe. (b) AFM topographic image of spin-coated bitumen surface and (c) surface force profile between an air bubble and bitumen in 1 mmol·L^{-1} NaCl at pH 4.0. (d–f) AFM images of bitumen surfaces in 500 mmol·L^{-1} NaCl at (d) pH 4.0, (e) pH 5.8, and (f) pH 8.5. (g–i) Surface force profiles between air bubbles and bitumen in 500 mmol·L^{-1} NaCl at (g) pH 4.0, (h) pH 5.8, and (i) pH 8.5. (j) AFM image of bitumen surface and (k) force profile between an air bubble and bitumen in 500 mmol·L^{-1} NaCl + 10 mmol·L^{-1} $CaCl_2$ at pH 8.5. All the force measurements were conducted at a driven velocity of v = 1 μm·s^{-1} (symbols indicate experimental data and solid lines indicate theoretical analysis). Reproduced from Ref. [19] with permission.

provide some examples from our previous studies to show how the forces involved in emulsion interactions can be quantified using the relevant nanomechanical technologies.

The stabilization and destabilization of emulsions in petroleum production are highly relevant to the adsorption of interface-active species (e.g., natural surfactants, asphaltenes, and fine solids) to

oil/water interfaces, which can significantly change the interfacial properties (e.g., interfacial tension and interfacial rheology) and influence the surface interactions of emulsion droplets. Asphaltenes are commonly accepted as a typical interface-active species that contributes to the stabilization of emulsions in petroleum production. The interaction forces between two oil droplets with and without asphaltenes in different aqueous solutions were quantified by means of the drop probe AFM technique, as illustrated in Fig. 6(a) [64]. In an aqueous solution of 1 mmol·L^{-1} NaCl, repulsive forces were measured between two bare oil (toluene) droplets without asphaltenes. No drop coalescence was detected (Fig. 6(b)), mostly due to the EDL repulsion between the two oil droplets. In comparison, oil droplets containing asphaltenes exhibited stronger repulsive forces due to their significantly enhanced EDL interaction, which was caused by the oil/water interface being more negatively charged due to asphaltene adsorption (Figs. 6(b) and (c)). In contrast, in an aqueous solution of high salinity (100 mmol·L^{-1} NaCl), two bare oil droplets coalesced due to the significantly suppressed EDL repulsion and the attractive VDW interaction (Fig. 6(d)); however, the coalescence behavior was inhibited by the addition of asphaltenes (Fig. 6(e)), due to the strong steric forces between asphaltenes at the interface. Interestingly, by introducing an additional 10 mmol·L^{-1} Ca^{2+} to the 100 mmol·L^{-1} NaCl solution, the two oil droplets with asphaltenes were also able to coalesce. This phenomenon was most likely caused by the interactions of Ca^{2+} ions and certain groups on asphaltene molecules (i.e., carboxyl groups), which weakened the steric repulsion and facilitated the stabilization of the oil-in-water emulsion drops (Fig. 6(f)).

The drop probe AFM technique can also be used to measure the forces of two water-in-oil emulsion droplets, as illustrated in Fig. 7(a). When a water droplet approached another water droplet in an oil medium (i.e., toluene), the droplets exhibited behavior similar to that of the two oil droplets in an aqueous solution, and could readily coalesce after overcoming the very weak hydrodynamic repulsion (Fig. 7(b)) [65]. However, introducing asphaltenes to the oil phase efficiently suppressed such coalescence behavior (Fig. 7(c)), mainly because of the strong steric repulsive force arising from the asphaltene films adsorbed at the oil/water interface. It is also worth noting that adhesion was measured during the retraction process of the water droplets in 100 ppm of asphaltenes-in-toluene solution; this was believed to be due to interdigitation and interpenetration, as well as the aggregation of interfacial asphaltenes due to complex molecular interactions such as π–π stacking, acid–base interactions, and hydrogen bonding [65]. To better understand the emulsion interactions, the intermolecular interactions among the interface-active species (i.e., asphaltenes) at the oil/water interfaces were directly quantified using an SFA, as illustrated in Fig. 7(d) [14]. We found that the solvent condition significantly affects the interactions of asphaltenes. For two asphaltene surfaces interacting in pure *n*-heptane (a poor solvent for asphaltenes), in which the asphaltenes would be in a compressed and non-swelling conformation, a strong adhesive force was detected, as shown in Fig. 7(e). As the toluene weight ratio (ω) in heptol (a mixture of toluene and heptane) increased from 0 to 1, the adhesion measured between two asphaltene surfaces gradually decreased, and only weak repulsion (no adhesion) was detected in toluene, as shown in Fig. 7(f). These results can be explained as follows: The asphaltene molecules/nanoaggregates had a stronger tendency to be in a swelling conformation in a relatively good solvent (i.e., heptol with higher toluene fractions), which led to increased steric repulsion between the opposing swelling asphaltene surfaces [14]. It should be noted that the external flow conditions have a significant impact on the hydrodynamic interactions of emulsion systems, which can drastically affect the interactions among emulsions at large separation distances. Thus,

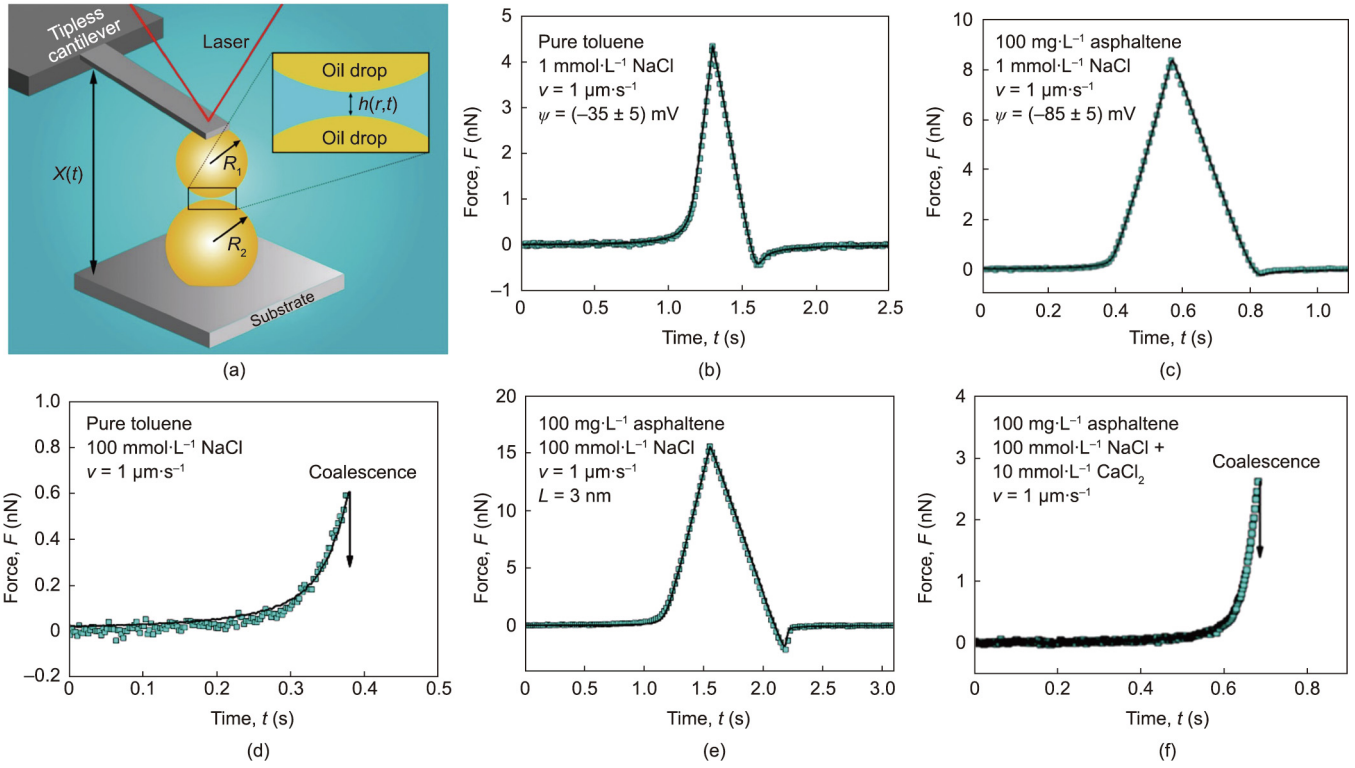

Fig. 6. (a) Illustration of the surface force measurement of two oil droplets in an aqueous medium using a drop probe based on AFM. (b–f) Force profiles for the interactions of two toluene droplets in (b) 1 mmol·L^{-1} NaCl without asphaltenes, (c) 1 mmol·L^{-1} NaCl with 100 mg·L^{-1} asphaltenes, (d) 100 mmol·L^{-1} NaCl without asphaltenes, (e) 100 mmol·L^{-1} NaCl with 100 mg·L^{-1} asphaltenes, and (f) 100 mmol·L^{-1} NaCl + 10 mmol·L^{-1} $CaCl_2$ with 100 mg·L^{-1} asphaltenes at a driven velocity of 1 μm·s^{-1}. The blue circles represent experimental data, while the solid black curves indicate theoretical analysis. Reproduced from Ref. [64] with permission.

to completely understand the emulsion interactions in the relevant petroleum production process, characterizing and understanding the hydrodynamic interactions is also of great importance. A computer-controlled four-roll mill fluidic device was fabricated in our lab and reported in a previous work to characterize the effects of external flow conditions on the emulsion interactions [14].

5. Fouling/antifouling issues and water treatment

Various components (e.g., asphaltenes, emulsions, and fine solids) in crude oil and production fluid media can interact with different substrate surfaces (e.g., pipelines and heat exchangers) during extraction, transportation, and other processes, which can cause many challenging issues such as fouling phenomena and environmental concerns. Thus, characterizing the interaction forces involved in the phenomena relevant to fouling/antifouling issues and water treatment is of great significance. The interaction forces between oil droplets and different solid substrates with various interface-active species (e.g., asphaltenes) can be quantitatively measured by means of the drop probe AFM technique, as illustrated in Fig. 8(a) [18].

When an oil (toluene) droplet with 10 mg·L^{-1} of asphaltenes approached a hydrophobized mica substrate using octadecyltrichlorosilane (OTS) (with a static water contact θ_w = 120° in toluene) in 100 mmol·L^{-1} NaCl, "jump-in" behavior was observed, as shown in Fig. 8(b). It should be noted that the Debye length was only 0.96 nm under the above solution conditions, so the EDL interaction would be significantly suppressed. A theoretical analysis using the SRYL model, which takes into account the contribution of hydrophobic interactions, is shown as the solid curve in Fig. 8(b), and agrees well with the experimental measurements. The expression for the exponential relation of the hydrophobic interaction potential between a liquid oil droplet and a flat hydrophobic substrate (an asymmetric configuration) (W_{HB}) is given by Eq. (13), and the disjoining pressure is given by Eq. (14), where θ_w is the static water contact angle on the hydrophobic substrate in oil, γ is the oil/water interfacial tension, and D_0 is the decay length of the hydrophobic interaction (D_0 = 1 nm in Fig. 8(b)) [32,44,66]. Thus, such attachment behavior is mainly driven by the hydrophobic interaction between the oil droplet and the hydrophobized mica by overcoming the steric interaction from the interfacial asphaltenes, resulting in strong attraction and attachment of the oil droplet to the hydrophobic substrate.

$$W_{HB}(h) = -\gamma(1 - \cos\theta_w)\exp(-h/D_0) \quad (13)$$

$$\prod_{HB}(h) = -\gamma(1 - \cos\theta_w)/D_0\exp(-h/D_0) \quad (14)$$

In contrast, "jump-in" behavior was not detected when an oil (toluene) droplet with 10 mg·L^{-1} of asphaltenes approached a hydrophilic mica surface under the same solution conditions (i.e., 100 mmol·L^{-1} NaCl), as shown in Fig. 8(c); this was mainly due to the steric hindrance of the asphaltenes adsorbed at the oil/water interface (forming a protective layer around the emulsion droplet). When increasing the applied load to compress the oil droplet containing 10 mg·L^{-1} of asphaltenes against the hydrophilic mica substrate, a weak adhesion force (about 5 nN) was detected, but the oil droplet could be fully detached from the mica substrate, suggesting a partial attachment of the oil droplet to the mica, as shown in the extraction force curve in Fig. 8(c). It was notable that, by increasing the asphaltene concentration in the oil phase to 100 mg·L^{-1} or higher, the oil drop–mica attachment behavior could be completely

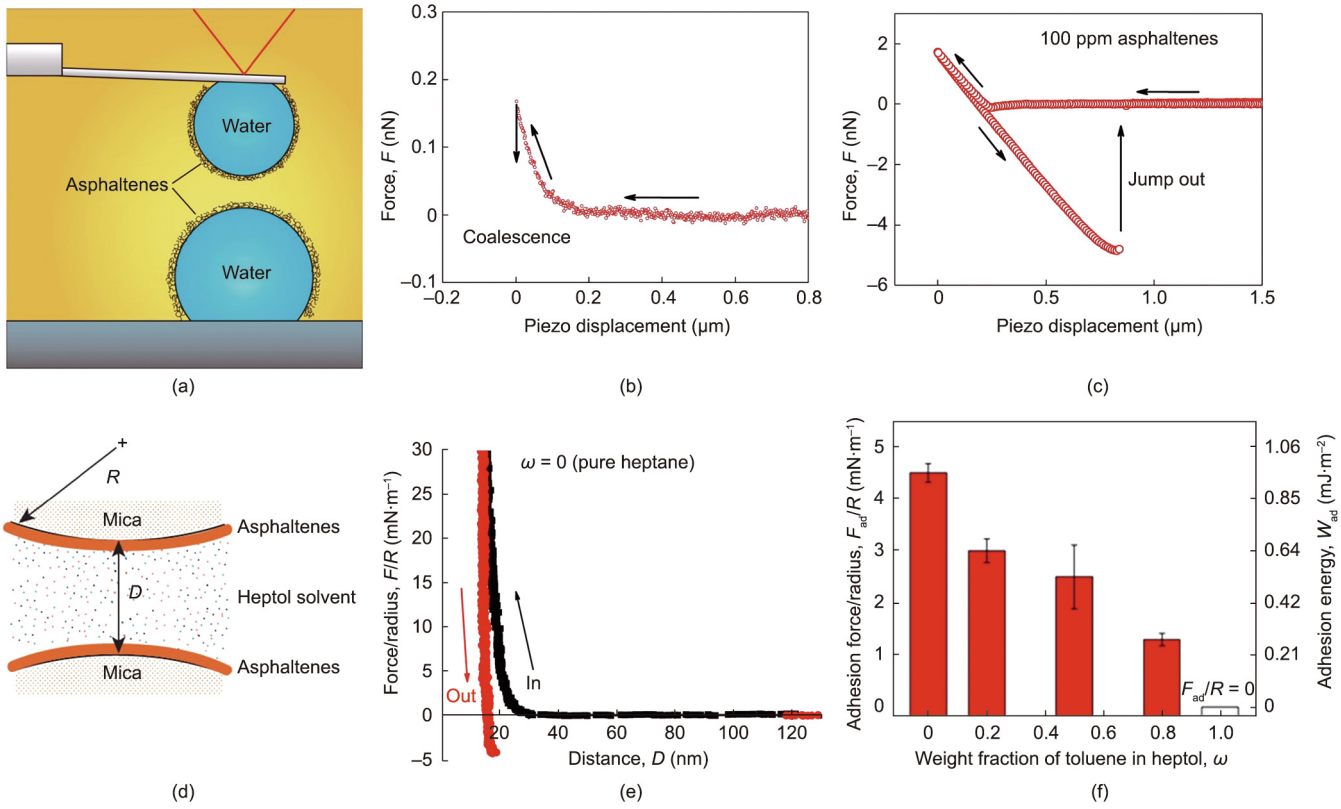

Fig. 7. (a) Illustration of the surface force measurement of two water droplets in an oil medium using a drop probe based on AFM. Reproduced from Ref. [15] with permission. (b, c) Measured force profiles of two water droplets interacting in toluene (b) with 0 ppm asphaltene and (c) with 100 ppm asphaltene. Reproduced from Ref. [65] with permission. (d) Illustration of SFA force measurements for asphaltenes versus asphaltenes in a liquid medium. (e) Measured force profiles for asphaltenes–asphaltenes interaction in pure *n*-heptane. (f) Normalized adhesion (F_{ad}/R, adhesion force/radius of the curved surface) and adhesion energy (W_{ad}) measured in heptol solvents with various toluene weight fractions (ω), as measured by SFA. (d–f) Reproduced from Ref. [14] with permission.

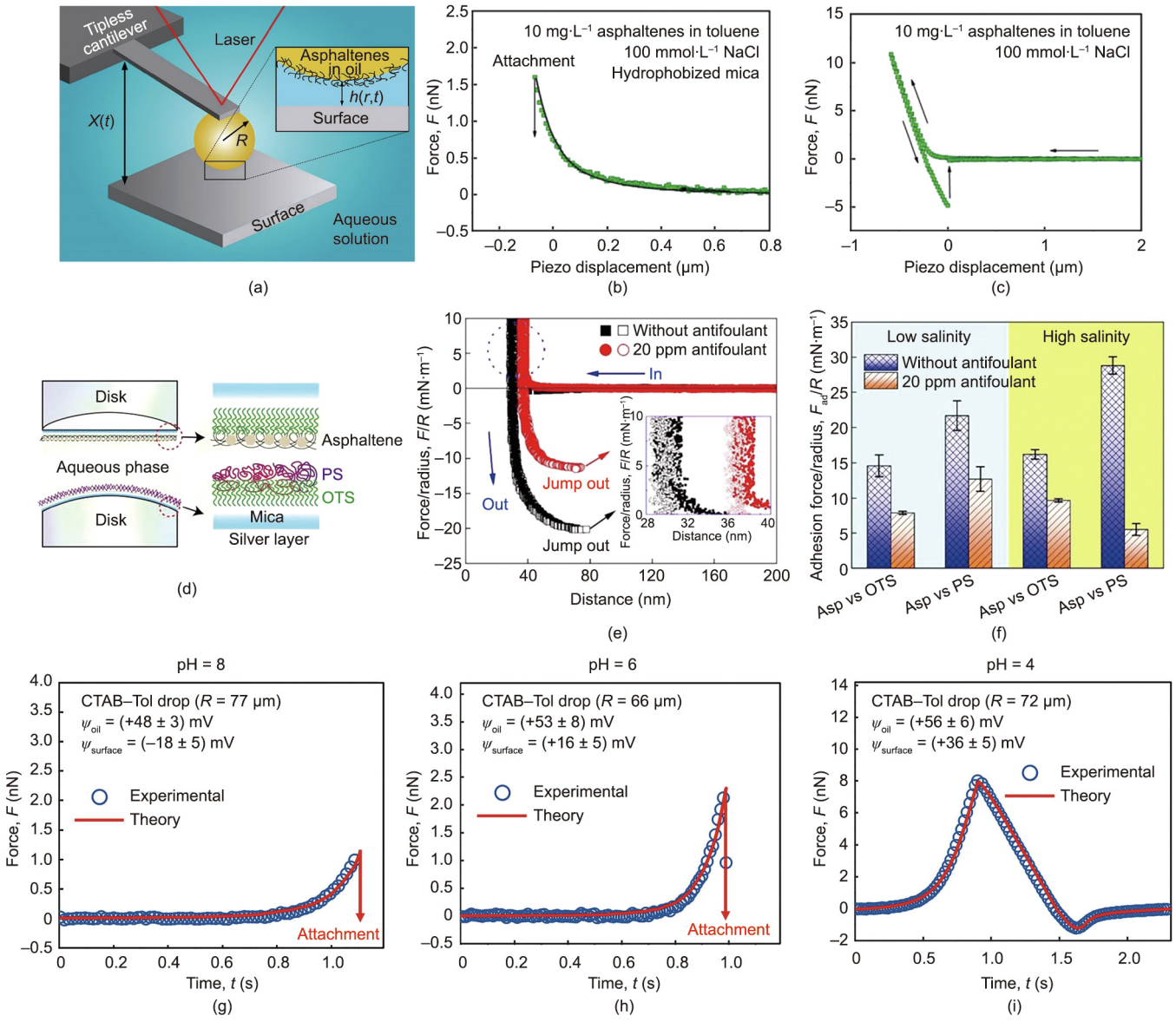

Fig. 8. (a) Schematic of the surface force measurement of an oil droplet and a solid surface in an aqueous solution using a drop probe based on AFM. (b, c) Measured force profiles (b) between an oil (toluene) droplet containing 10 mg·L^{-1} of asphaltenes and a hydrophobized mica surface and (c) between an oil droplet containing 10 mg·L^{-1} of asphaltenes and a hydrophilic mica surface in 100 mmol·L^{-1} NaCl. Green symbols represent experimental data, while black lines indicate theoretical analysis results. (a–c) Reproduced from Ref. [18] with permission. (d) Schematic of the surface force measurement between asphaltenes and polystyrene (PS) using an SFA. (e) Force–distance curves for asphaltene–PS interactions with and without 20 ppm of antifoulant. (f) Adhesion detected for asphaltene–OTS and asphaltene (Asp)–PS interactions under different conditions of low/high salinity and with/without 20 ppm of antifoulant. (d–f) Reproduced from Ref. [67] with permission. (g–i) Measured force profiles (open symbols) of an oil droplet (toluene, Tol) containing 200 ppm of cetrimonium bromide (CTAB) with a polydopamine (PDA)–poly(acrylic acid) (PAA)–poly[2-(methacryloyloxy) ethyltrimethylammonium chloride] (PMTAC) polymer surface in 1 mmol·L^{-1} of NaCl under different pH conditions of (g) pH 8, (h) pH 6, and (i) pH 4. Red solid curves indicate theoretical analysis. (g–i) Reproduced from Ref. [68] with permission.

suppressed. Under high asphaltene concentration, more asphaltenes migrated to the interface, forming a strong protective layer and causing very strong steric interaction against the hydrophilic mica surface, which was strongly hydrated with water and adsorbed with hydrated cations (e.g., Na^+) in the Stern layer of the EDL. Such strong steric interaction inhibited the attachment of the oil drop to the hydrophilic mica. These results provide very useful information on the intermolecular and surface interaction mechanisms underlying the phenomena of fouling and antifouling.

To understand the physical mechanisms underlying the fouling and antifouling phenomena of asphaltenes on different substrates and the influence of antifoulants, we employed an SFA and quantified the forces of asphaltenes with two model hydrophobic substrates (i.e., OTS and polystyrene (PS)), in the absence and presence of a commercial quaternary ammonium-based polymer antifoulant, as shown in Fig. 8(d) [67]. Force measurements were conducted under both low salinity conditions (i.e., 160 ppm NaCl and 20 ppm KCl, as model process water for the *in situ* extraction of bitumen from oil sands) and high salinity conditions (i.e., 1 mol·L^{-1} NaCl). For the low salinity case, the PS–asphaltenes adhesion was measured as about 22 mN·m^{-1} if no antifoulant was added, which was mainly attributed to their hydrophobic and VDW interactions. In contrast, upon introducing 20 ppm of antifoulant to the aqueous solution, the adhesion was significantly reduced to approximately 13 mN·m^{-1}, as shown in Fig. 8(e). It was also noted that the hard wall separation distance was shifted from about 30 nm to about 38 nm when 20 ppm of antifoulant was added. These results indicate that the antifoulant was able to adsorb to the surfaces to lower the adhesion of the organics to hydrophobic substrates in order to achieve the observed antifoul-

ing performance. The surface forces of asphaltenes with OTS and PS (as model hydrophobic substrates) under both low and high salinity conditions were also systematically quantified using an SFA, and the results are summarized and shown in Fig. 8(f). Without antifoulant, the EDL forces could be significantly screened in the high-salinity solution; thus, the adhesion measured was found to be stronger than that of the low-salinity case. Upon introducing the antifoulant, the adhesion was weakened under both high-salinity and low-salinity solution conditions, with a more significant drop for the high-salinity case (Fig. 8(f)). These experiments demonstrated the excellent antifouling performance of the antifoulants via weakening the adhesion between potential foulants (e.g., asphaltenes) and the model substrate surfaces. These nanomechanical measurements reveal the underlying intermolecular interaction mechanisms associated with the fouling and antifouling phenomena, facilitating the development of efficient antifoulants for the petroleum industry and relevant engineering processes.

Process water and tailings water in petroleum engineering should be properly treated before their cyclic use in petroleum production or being discharged to the environment. Various technologies can be used for this purpose, such as membrane filtration, flocculation and coagulation via the addition of chemical additives (e.g., flocculants or coagulants), and dissolved air flotation (for removing oil residues and some hydrophobic solids). The efficiency of these water treatment processes is highly dependent on how the molecules, particles, oil droplets, and gas bubbles interact in aqueous media. Thus, revealing the relevant interfacial interaction mechanisms is of great significance. Taking the interfacial interactions involved in membrane filtration progresses as an example, in a recent work, we reported a type of bio-inspired antifouling coating composed of carboxyl and quaternary ammonium groups. The bio-inspired coating exhibited antifouling properties that could be adapted or tuned by tuning the surface interactions—particularly the EDL interactions—between the coating surface and the emulsion droplets in the surrounding fluid media [68]. Figs. 8(g)–(i) shows the results from the surface force measurements of toluene droplets containing 200 ppm of cetrimonium bromide (CTAB) and polydopamine (PDA)–poly(acrylic acid) (PAA)–poly[2-(methacryloyloxy)ethyltrimethylammonium chloride] (PMTAC) coating in 1 mmol·L^{-1} of NaCl under various pH conditions. "Jump-in" behavior was detected when a toluene droplet containing 200 ppm of CTAB approached a PDA–PAA–PMTAC coating at pH 8 and pH 6. In contrast, at pH 4, no attachment of the oil drop to the polymer coating was observed. Lowering the solution pH from 8 to 4 changed the PDA–PAA–PMTAC surface from being negatively charged (surface potential = −18 mV) to positively charged (surface potential = +36 mV), thus tuning the EDL forces with toluene droplets. However, the VDW and hydrodynamic interactions were barely influenced when varying the aqueous pH. Thus, the overall interactions of oil drops and PDA–PAA–PMTAC changed from attraction at high pH (i.e., pH 8) to weak attraction at intermediate pH (i.e., pH 6) and to pure repulsion at low pH (i.e., pH 4). These results demonstrate that varying the solution pH can facilely tune the surface charges of the PDA–PAA–PMTAC coating and then effectively affect its surface forces with the oil droplets. These intermolecular and surface force measurements provide valuable insights into emulsion-related fouling phenomena in petroleum production and the fabrication of new membranes or surfaces with excellent antifouling performance toward efficient oily water treatment.

6. Conclusions and perspectives

The performance and efficiency of petroleum operations are significantly driven and influenced by the forces among the different oil components, water, mineral solids, chemical additives, and gas bubbles involved in the relevant surrounding fluid media under specific environmental conditions. Herein, we presented our recent progress in probing various interfacial interactions involved in several typical petroleum production processes such as oil extraction (particularly bitumen extraction from oil sands), emulsion stabilization and destabilization, fouling phenomena and antifouling strategies (antifoulant additives and antifouling surfaces), and water treatment. Commonly used nanomechanical tools including the SFA and AFM (coupled with a sharp probe, colloid probe, and bubble or drop probe, and with RICM) were introduced, which allow the direct quantification of the interfacial forces involved in relevant petroleum production processes. The classical DLVO theory was adopted to explain the general trends of the interaction behaviors of emulsion drops and solid particles in a fluid medium in petroleum production, in terms of the VDW and EDL forces involved. However, because of the complex operation and environmental conditions involved in crude oil extraction (e.g., solution chemistry, temperature, and pressure), the complexity of the molecular structures of various components in crude oil, and the influence of the hydrodynamic interactions on the emulsion systems, the molecular chemistries and compositions of crude oil are still largely unknown despite the considerable amount of progress that has been achieved. Thus, the DLVO theory often fails to describe the full picture of the colloidal interactions involved in a petroleum production process. Therefore, other intermolecular and interfacial interactions such as hydrophobic, solvation (e.g., hydration), steric, and aromatic interactions should be considered and included in the analysis of the force profiles obtained. By using nanomechanical tools (i.e., SFA and AFM), we have quantified the forces among bitumen, mineral solids, asphaltenes, oil/water emulsions, and chemical additives (i.e., antifoulants) in different aqueous or organic solutions. The impact of aqueous conditions (i.e., salinity, ion type, and pH in aqueous solutions), interface-active species, and solvent types (i.e., a varying ratio of good and poor organic solvents) on these intermolecular and interfacial interaction behaviors was also investigated and discussed, providing useful information on how environmental conditions impact these interactions in relevant petroleum production processes.

Although much progress has been achieved, a complete picture of the interfacial interactions involved in petroleum production has not been achieved, mainly due to the complex molecular chemistries of crude oil and the environmental conditions in practical operations, as mentioned above. Characterizing the molecular structures and expanding the relevant database of complex petroleum components are very important research directions in petroleum engineering, and future research will focus more on correlating the interfacial forces of petroleum species having clearly defined structures with their characteristics and properties in practical petroleum production processes. Many tools such as the SFA and AFM allow force measurements at elevated temperature conditions (e.g., up to about 60–80 °C). However, it has been generally experimentally difficult to apply nanomechanical tools (e.g., SFA, AFM, and OT) to measure the intermolecular and surface forces of petroleum components under high temperature (> 100 °C), high pressure, and even highly corrosive solution conditions, which are commonly encountered in practical petroleum production operations. Further developing nanomechanical techniques and accessories that can accommodate force measurements under the abovementioned harsh environmental conditions will enable the exploration of the molecular forces and interfacial interactions in practical petroleum production processes. In short, direct measurements of the molecular and interfacial forces of various objects in petroleum production processes provide valuable insights into the working principles of these engineering processes, facilitating the exploitation of innovative materials and surfaces, as

well as improved interfacial processes to support the sustainable development of natural resources.

Acknowledgments

This work was supported by the Natural Sciences and Engineering Research Council of Canada (NSERC), the Canada Foundation for Innovation (CFI), the Research Capacity Program (RCP) of Alberta, the Future Energy Systems under the Canada First Research Excellence Fund, and the Canada Research Chairs Program.

Compliance with ethics guidelines

Diling Yang, Xuwen Peng, Qiongyao Peng, Tao Wang, Chenyu Qiao, Ziqian Zhao, Lu Gong, Yueliang Liu, Hao Zhang, and Hongbo Zeng declare that they have no conflict of interest or financial conflicts to disclose.

References

[1] Masliyah JH, Czarnecki J, Xu Z. Handbook on theory and practice on bitumen recovery from Athabasca oil sands. Menlyn: Kingsley Publishing Services; 2011.
[2] Masliyah J, Zhou ZJ, Xu Z, Czarnecki J, Hamza H. Understanding water-based bitumen extraction from Athabasca oil sands. Can J Chem Eng 2004;82(4):628–54.
[3] Butler RM. Steam-assisted gravity drainage: concept, development, performance and future. J Can Pet Technol 1994;33(2):44–50.
[4] Pushkarova RA, Horn RG. Surface forces measured between an air bubble and a solid surface in water. Colloids Surf A Physicochem Eng Asp 2005;261(1–3):147–52.
[5] Tabor D, Winterton RHS. The direct measurement of normal and retarded van der Waals forces. Proc R Soc Lond A Math Phys Sci 1969;312(1511):435–50.
[6] Israelachvili JN, Tabor D. The measurement of van der Waals dispersion forces in the range 1.5 to 130 nm. Proc R Soc Lond A Math Phys Sci 1972;331(1584):19–38.
[7] Israelachvili JN, Adams GE. Direct measurement of long range forces between two mica surfaces in aqueous KNO_3 solutions. Nature 1976;262(5571):774–6.
[8] Israelachvili J, Min Y, Akbulut M, Alig A, Carver G, Greene W, et al. Recent advances in the surface forces apparatus (SFA) technique. Rep Prog Phys 2010;73(3):036601.
[9] Binnig G, Quate CF, Gerber C. Atomic force microscope. Phys Rev Lett 1986;56(9):930–3.
[10] Ashkin A. Acceleration and trapping of particles by radiation pressure. Phys Rev Lett 1970;24(4):156–9.
[11] Ashkin A, Dziedzic JM, Bjorkholm JE, Chu S. Observation of a single-beam gradient force optical trap for dielectric particles. Opt Lett 1986;11(5):288–90.
[12] Derjaguin B, Rabinovich YI, Churaev N. Direct measurement of molecular forces. Nature 1978;272(5651):313–8.
[13] Butt HJ, Jaschke M, Ducker W. Measuring surface forces in aqueous electrolyte solution with the atomic force microscope. Bioelectrochem Bioenergy 1995;38(1):191–201.
[14] Zhang L, Shi C, Lu Q, Liu Q, Zeng H. Probing molecular interactions of asphaltenes in heptol using a surface forces apparatus: implications on stability of water-in-oil emulsions. Langmuir 2016;32(19):4886–95.
[15] Shi C, Zhang L, Xie L, Lu X, Liu Q, He J, et al. Surface interaction of water-in-oil emulsion droplets with interfacially active asphaltenes. Langmuir 2017;33(5):1265–74.
[16] Liu J, Cui X, Huang J, Xie L, Tan X, Liu Q, et al. Understanding the stabilization mechanism of bitumen-coated fine solids in organic media from non-aqueous extraction of oil sands. Fuel 2019;242:255–64.
[17] Gong L, Zhang L, Xiang L, Zhang J, Fattahpour V, Mamoudi M, et al. Surface interactions between water-in-oil emulsions with asphaltenes and electroless nickel–phosphorus coating. Langmuir 2020;36(4):897–905.
[18] Shi C, Xie L, Zhang L, Lu X, Zeng H. Probing the interaction mechanism between oil droplets with asphaltenes and solid surfaces using AFM. J Colloid Interface Sci 2020;558:173–81.
[19] Xie L, Shi C, Cui X, Huang J, Wang J, Liu Q, et al. Probing the interaction mechanism between air bubbles and bitumen surfaces in aqueous media using bubble probe atomic force microscopy. Langmuir 2018;34(3):729–38.
[20] Liu J, Xu Z, Masliyah J. Studies on bitumen–silica interaction in aqueous solutions by atomic force microscopy. Langmuir 2003;19(9):3911–20.
[21] Kegler K, Salomo M, Kremer F. Forces of interaction between DNA-grafted colloids: an optical tweezer measurement. Phys Rev Lett 2007;98(5):058304.
[22] He L, Lin F, Li X, Sui H, Xu Z. Interfacial sciences in unconventional petroleum production: from fundamentals to applications. Chem Soc Rev 2015;44(15):5446–94.
[23] Drummond C, Israelachvili J. Fundamental studies of crude oil–surface water interactions and its relationship to reservoir wettability. J Petrol Sci Eng 2004;45(1–2):61–81.
[24] Christenson HK, Israelachvili JN. Direct measurements of interactions and viscosity of crude oils in thin films between model clay surfaces. J Colloid Interface Sci 1987;119(1):194–202.
[25] Chen SY, Kaufman Y, Kristiansen K, Seo D, Schrader AM, Alotaibi MB, et al. Effects of salinity on oil recovery (the "dilution effect"): experimental and theoretical studies of crude oil/brine/carbonate surface restructuring and associated physicochemical interactions. Energy Fuels 2017;31(9):8925–41.
[26] Natarajan A, Xie J, Wang S, Liu Q, Masliyah J, Zeng H, et al. Understanding molecular interactions of asphaltenes in organic solvents using a surface force apparatus. J Phys Chem C 2011;115(32):16043–51.
[27] Zhang J, Zeng H. Intermolecular and surface interactions in engineering processes. Engineering 2020;7(1):63–83.
[28] Schäffer E, Nørrelykke SF, Howard J. Surface forces and drag coefficients of microspheres near a plane surface measured with optical tweezers. Langmuir 2007;23(7):3654–65.
[29] Lu Q, Wang J, Faghihnejad A, Zeng H, Liu Y. Understanding the molecular interactions of lipopolysaccharides during *E. coli* initial adhesion with a surface forces apparatus. Soft Matter 2011;7(19):9366–79.
[30] Butt HJ, Cappella B, Kappl M. Force measurements with the atomic force microscope: technique, interpretation and applications. Surf Sci Rep 2005;59(1–6):1–152.
[31] Israelachvili JN. Measurement of forces between surfaces immersed in electrolyte solutions. Faraday Discuss Chem Soc 1978;65:20–4.
[32] Israelachvili J, Pashley R. The hydrophobic interaction is long range, decaying exponentially with distance. Nature 1982;300(5890):341–2.
[33] Zhang J, Xiang L, Yan B, Zeng H. Nanomechanics of anion—ΠI interaction in aqueous solution. J Am Chem Soc 2020;142(4):1710–4.
[34] Lu Q, Oh DX, Lee Y, Jho Y, Hwang DS, Zeng H. Nanomechanics of cation–π interactions in aqueous solution. Angew Chem 2013;125(14):4036–40.
[35] Zhang L, Xie L, Shi C, Huang J, Liu Q, Zeng H. Mechanistic understanding of asphaltene surface interactions in aqueous media. Energy Fuels 2017;31(4):3348–57.
[36] Faghihnejad A, Zeng H. Hydrophobic interactions between polymer surfaces: using polystyrene as a model system. Soft Matter 2012;8(9):2746–59.
[37] Xiang Li, Gong Lu, Zhang J, Zhang L, Hu W, Wang W, et al. Probing molecular interactions of PEGylated chitosan in aqueous solutions using a surface force apparatus. Phys Chem Chem Phys 2019;21(37):20571–81.
[38] Israelachvili JN. Thin film studies using multiple-beam interferometry. J Colloid Interface Sci 1973;44(2):259–72.
[39] Drake B, Prater CB, Weisenhorn AL, Gould SAC, Albrecht TR, Quate CF, et al. Imaging crystals, polymers, and processes in water with the atomic force microscope. Science 1989;243(4898):1586–9.
[40] Zeng H. Polymer adhesion, friction, and lubrication. New York: John Wiley & Sons; 2013.
[41] Akamine S, Barrett RC, Quate CF. Improved atomic force microscope images using microcantilevers with sharp tips. Appl Phys Lett 1990;57(3):316–8.
[42] Yang D, Xie L, Mao X, Gong Lu, Peng X, Peng Q, et al. Probing hydrophobic interactions between polymer surfaces and air bubbles or oil droplets: effects of molecular weight and surfactants. Langmuir 2022;38(17):5257–68.
[43] Cui X, Liu J, Xie L, Huang J, Liu Q, Israelachvili JN, et al. Modulation of hydrophobic interaction by mediating surface nanoscale structure and chemistry, not monotonically by hydrophobicity. Angew Chem 2018;130(37):12079–84.
[44] Cui X, Shi C, Zhang S, Xie L, Liu J, Jiang D, et al. Probing the effect of salinity and ph on surface interactions between air bubbles and hydrophobic solids: implications for colloidal assembly at air/water interfaces. Chem Asian J 2017;12(13):1568–77.
[45] Gong Lu, Wang J, Zhang L, Fattahpour V, Mamoudi M, Roostaei M, et al. Fouling mechanisms of asphaltenes and fine solids on bare and electroless nickel-phosphorus coated carbon steel. Fuel 2019;252:188–99.
[46] Gong L, Qiu X, Zhang L, Huang J, Hu W, Xiang L, et al. Probing the interaction mechanism between oil-in-water emulsions and electroless nickel–phosphorus coating with implications for antifouling in oil production. Energy Fuels 2019;33(5):3764–75.
[47] Liu J, Cui X, Xie L, Huang J, Zhang L, Liu J, et al. Probing effects of molecular-level heterogeneity of surface hydrophobicity on hydrophobic interactions in air/water/solid systems. J Colloid Interface Sci 2019;557:438–49.
[48] Shi C, Chan DYC, Liu Q, Zeng H. Probing the hydrophobic interaction between air bubbles and partially hydrophobic surfaces using atomic force microscopy. J Phys Chem C 2014;118(43):25000–8.
[49] Xie L, Shi C, Wang J, Huang J, Lu Q, Liu Q, et al. Probing the interaction between air bubble and sphalerite mineral surface using atomic force microscope. Langmuir 2015;31(8):2438–46.
[50] Shi C, Cui X, Xie L, Liu Q, Chan DYC, Israelachvili JN, et al. Measuring forces and spatiotemporal evolution of thin water films between an air bubble and solid surfaces of different hydrophobicity. ACS Nano 2015;9(1):95–104.
[51] Qiao C, Yang D, Mao X, Xie L, Gong L, Peng X, et al. Recent advances in bubble-based technologies: underlying interaction mechanisms and applications. Appl Phys Rev 2021;8(1):011315.

[52] Ducker WA, Senden TJ, Pashley RM. Direct measurement of colloidal forces using an atomic force microscope. Nature 1991;353(6341):239–41.
[53] Ducker WA, Xu Z, Israelachvili JN. Measurements of hydrophobic and DLVO forces in bubble-surface interactions in aqueous solutions. Langmuir 1994;10(9):3279–89.
[54] Butt HJ. Measuring electrostatic, van der Waals, and hydration forces in electrolyte solutions with an atomic force microscope. Biophys J 1991;60(6):1438–44.
[55] Israelachvili JN. Intermolecular and surface forces. 3rd ed. New York City: Academic Press; 2011.
[56] Ivanov IB, Dimitrov DS, Somasundaran P, Jain RK. Thinning of films with deformable surfaces: diffusion-controlled surfactant transfer. Chem Eng Sci 1985;40(1):137–50.
[57] Stevens H, Considine RF, Drummond CJ, Hayes RA, Attard P. Effects of degassing on the long-range attractive force between hydrophobic surfaces in water. Langmuir 2005;21(14):6399–405.
[58] Manica R, Klaseboer E, Chan DYC. Dynamic interactions between drops—a critical assessment. Soft Matter 2008;4(8):1613–6.
[59] Manica R, Chan DYC. Drainage of the air–water–quartz film: experiments and theory. Phys Chem Chem Phys 2011;13(4):1434–9.
[60] Manor O, Vakarelski IU, Tang X, O'Shea SJ, Stevens GW, Grieser F, et al. Hydrodynamic boundary conditions and dynamic forces between bubbles and surfaces. Phys Rev Lett 2008;101(2):024501.
[61] Manor O, Vakarelski IU, Stevens GW, Grieser F, Dagastine RR, Chan DYC. Dynamic forces between bubbles and surfaces and hydrodynamic boundary conditions. Langmuir 2008;24(20):11533–43.
[62] Chan DYC, Klaseboer E, Manica R. Film drainage and coalescence between deformable drops and bubbles. Soft Matter 2011;7(6):2235–64.
[63] Liu J, Xu Z, Masliyah J. Colloidal forces between bitumen surfaces in aqueous solutions measured with atomic force microscope. Colloids Surf A Physicochem Eng Asp 2005;260(1–3):217–28.
[64] Shi C, Zhang L, Xie L, Lu X, Liu Q, Mantilla CA, et al. Interaction mechanism of oil-in-water emulsions with asphaltenes determined using droplet probe AFM. Langmuir 2016;32(10):2302–10.
[65] Xie L, Lu Q, Tan X, Liu Q, Tang T, Zeng H. Interfacial behavior and interaction mechanism of pentol/water interface stabilized with asphaltenes. J Colloid Interface Sci 2019;553:341–9.
[66] Cui X, Shi C, Xie L, Liu J, Zeng H. Probing interactions between air bubble and hydrophobic polymer surface: impact of solution salinity and interfacial nanobubbles. Langmuir 2016;32(43):11236–44.
[67] Qiao C, Wang D, Zhao Z, Yang W, Wu F, Chen H, et al. Bench-scale oil fouling/antifouling tests under high temperature and high pressure conditions and the underlying interfacial interaction mechanisms. Fuel 2022;314:122720.
[68] Pan M, Gong L, Xiang L, Yang W, Wang W, Zhang L, et al. Modulating surface interactions for regenerable separation of oil-in-water emulsions. J Membr Sci 2021;625:119140.